

Spiking ruby revisited: self-induced periodic spiking oscillations leading to chaotic state in a Cr:Al₂O₃ laser with cw 532-nm pumping

KENJU OTSUKA¹ AND SEIICHI SUDO²

¹*T³L Research, 126-7 Yamaguchi, Tokorozawa, Saitama 359-1145 Japan*

²*Department of Physics, Tokyo City University, Tokyo 158-8557 Japan*

*Corresponding author: kenju.otsuka@gmail.com

This paper reexamines a 60-year-old mystery of spiking behavior in ruby lasers with a cw 532-nm pump, paying special attention to mode matching between the pump and lasing beam within a ruby crystal placed in a semi-confocal laser cavity. Periodic spiking oscillations were observed in a limited pump power regime, where spikes obeying the generic asymmetric hyperbolic function appeared at a repetition rate around 50 kHz and with a 130-150-ns width and 0.1-0.6- μ J energy depending on the pump power. The physics of the spiking behavior based on Kleinman's mechanical approach and a plausible interpretation for the periodic spiking oscillation in terms of self-induced mode matching between the pump and laser beams through the self-induced Kerr-lens effect are addressed. The statistical nature inherent to spiking and the associated self-organized critical behavior in quasi-periodic spiking oscillations as well as chaotic states occurring outside the periodic spiking regime are also explored from a nonlinear dynamics point of view.

The tremendous progress that has been witnessed in the laser sciences and optical technologies all started with T. Maiman's ruby laser [1]. A few years after the development of the ruby laser, a certain problem was nearly forgotten until the advent of the Ar laser pumped cw ruby laser [2-6]. That is, when this laser was first demonstrated, its output was regarded as being completely stable under cw pumping at helium or nitrogen temperatures [2, 4]. Later, other investigators disagreed and reported dynamical instabilities [3, 5, 6]. It has become clear since then that ruby lasers can operate under both conditions. Not only can the laser be completely stable, but it can also operate in instability conditions of chaotic and regular pulsing output [7]. The repetitive self-switching as well as related undamped spiking phenomena still remain as interesting unsolved mysteries in ruby lasers. There is to date still no definite understanding of the physical mechanism driving the instability.

On the other hand, two-orders of spectral narrowing of the fluorescence line width is required by cooling the rod to liquid nitrogen temperatures for cw argon ion laser pumping at 514.5 nm. Recently, two research groups have realized room-temperature cw ruby lasers by pumping at the optimum of the absorption profile at 405 nm of GaN laser diodes [8, 9], where both employed ruby crystals with a Cr₂O₃ concentration of 0.05 % and a c-axis at 90° relative to the crystal axis. These cw ruby laser oscillations with GaN laser-diode pumping raise intriguing questions as to whether room-temperature LD pumping at 405 nm can solve the over 60-year-old mystery of the spiking behaviors in ruby lasers.

Here, we performed systematic experiments towards room-temperature cw operation of ruby lasers pumped with a frequency-doubled Nd:YAG laser at 532 nm. Unfortunately, non-spiking cw

oscillations were not achieved, while self-induced periodic spiking oscillations leading to quasi-periodic spiking and chaotic states were observed. The physics of the spiking behavior based on Kleinman's mechanical approach and a plausible interpretation for the periodic spiking oscillation in terms of self-induced mode matching between pump and laser beams are addressed.

The experimental setup is shown in Fig. 1(a). A TEM₀₀ second harmonic output (wavelength: 532 nm) of an LD-pumped linearly-polarized TEM₀₀ mode Nd:YAG laser (CNI MG-F-532; TEM₀₀ mode, M² = 1.2), whose polarization direction was set perpendicular to the ruby c-axis by a half-wave plate, was focused on a 7-mm-thick, 10-mm-diameter a-cut ruby single crystal (Cr³⁺:Al₂O₃) with a 0.03 wt% Cr concentration, while the absorption coefficient at 532 nm was measured to be $\alpha = 2.1 \text{ cm}^{-1}$. The end surface was directly coated with a dielectric mirror M₁ (transmission at 532 nm = 88%, reflectance at 694 nm = 99.8%). A concave mirror M₂ (reflectance at 694 nm = 99%; radius of curvature, R₂ = 5 cm) was placed nearly 2.5 cm in optical length apart from the mirror M₁ to form the most stable semi-confocal laser cavity. The pump beam spot size averaged over the crystal was made close to the semi-confocal cavity spot size (around 70 μ m) by controlling the pump beam diameter at the lens of focal length f = 15 cm for decreasing the threshold pump power. The lasing pattern was measured by a mode profiler and the output was detected by a Si photo-diode (New Focus 1801M, 125 MHz bandwidth) followed by a digital oscilloscope (Tektronix DPO 2024, 200-MHz bandwidth).

The input-output characteristics are shown in Fig. 1(b), where the far-field lasing pattern exhibited a TEM₀₀ transverse mode as shown in the inset. The dynamic

behavior was found to change with increasing pump power, as depicted in Fig. 1(b). Periodic spiking oscillations appeared in the limited pump power regime, PS, while the periodicity was undermined in the lower pump region, QS, featuring quasi-periodicities and a chaotic state appeared in the higher pump regime, CS, above the PS regime. An example of a periodic spiking oscillation is shown in Fig. 2(a), together with the corresponding power spectrum and Poincaré section. The pump-dependent repetition frequency, spike pulse width, and associated spike-energy are shown in Fig. 2(b), where the peak output power was calibrated from the averaged output power shown in Fig. 1(b). The peak power of spikes within the cavity reached 100~400W, reflecting extremely low duty cycles of 0.6~0.75%.

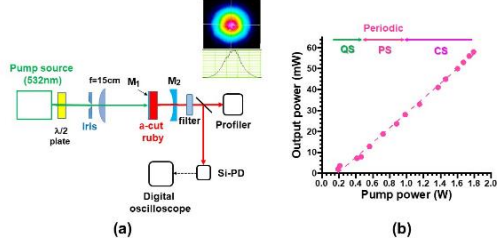


Fig. 1. (a) Experimental apparatus. (b) Input-output characteristics. QS: quasi-periodic spiking regime, PS: periodic spiking regime, CS: chaotic state.

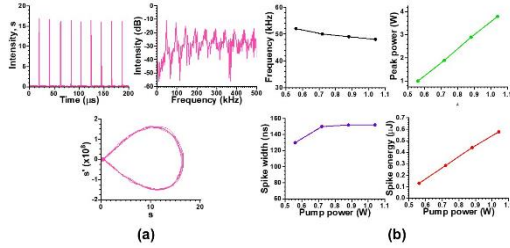


Fig. 2. Periodic spiking oscillation. (a) waveform, power spectrum, and Poincaré section at pump power of $P = 1040$ mW. (b) Pump-dependent repetition frequency, peak power, pulse width and energy of spiking pulse.

Results for the quasi-periodic spiking and chaotic state are summarized in Fig. 3.

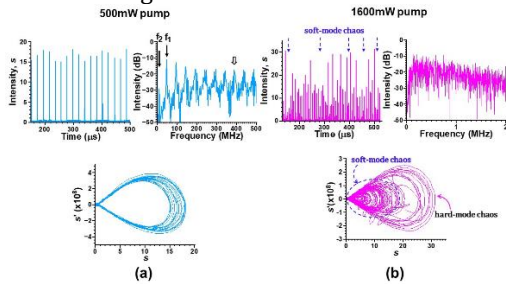


Fig. 3. (a) Quasi-periodic spiking oscillation featuring two competing frequencies, $f_1 = 9.5$ kHz and $f_2 = 48.75$ kHz, whose higher harmonic components merge in the vicinity of 390 kHz. (b) Chaotic state featuring alternating soft and hard-mode chaos over time.

To provide physical insight into the periodic excitation of the spiking oscillations, let us introduce the Toda potential for the laser rate equations. According to Kleiman's mechanical approach relevant to four-level as well as three-level systems like a ruby laser, which are governed by standard rate equations for population inversions and photon density [10-12], the dynamics of the photon

density can be understood in analogy with the motion of a particle in the following laser Toda potential, V , with a logarithmic transformation for the photon density as $u(t) \equiv \ln s(t)$ [12]:

$$d^2u/dt^2 + \kappa(du/dt) + \partial V/\partial u = F_D(t), \quad (1)$$

$$V = K[(e^u - 1) - (w - 1)u], \quad (2)$$

$$\kappa = 1 + e^u, \quad (3)$$

where $w = P/P_{th}$ (P : pump power, P_{th} : threshold pump power), $K = \tau/\tau_p$ (τ : fluorescence lifetime, τ_p : photon lifetime), F_D is a driving force to the particle, while the effect of spontaneous emission is neglected for the sake of brevity. The pump-dependent laser Toda potentials [13], $V(u)$, are shown in Fig. 4(a). The particle moves within a highly asymmetric laser Toda potential with a damping rate, κ .

Without a driving force, F_D , in Fig. 4(a), the particle approaches the ground state, exhibiting damped relaxation oscillations. Hamiltonian motion around the ground state, i.e., periodic relaxation oscillations (soft mode), is established if a periodic driving force is applied at the relaxation oscillation frequency, $f_{RO} = (1/2\pi)[(w - 1)/\tau\tau_p]^{1/2}$, such that the damping force, $\kappa(du/dt)$, balances the periodic driving force, F_D [12]. In addition to the soft mode, a spike-like waveform builds up within the asymmetric potential by tuning the strength and frequency of the driving force in the large signal regime. In fact, periodic spiking oscillations (hard-mode) were realized in semiconductor lasers through the use of deep injection current modulation [14] and in solid-state lasers through the use of a deep pump [15] or loss modulation [12] at $f_{SP} (< f_{RO})$ as well as delayed incoherent feedback [16].

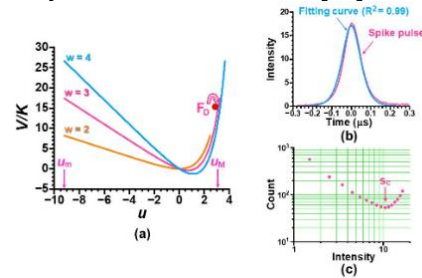


Fig. 4. (a) Pump-dependent laser Toda potentials. $w = P/P_{th}$. (b) Zoomed-in view of spike waveform, together with the hyperbolic fitting curve. (c) Intensity probability distribution for periodic spiking oscillations shown in Fig. 2 (a).

Let us examine whether the self-induced periodic spiking oscillations shown in Fig. 2(a) obey the generic dynamic properties of spiking oscillations reported so far. The spike-pulse waveform is confirmed to be well fitted by the following hyperbolic function, as in [12]:

$$s(t) = s_p \operatorname{sech}^2 \left(\sqrt{\frac{s_p}{2\tau\tau_p}} (t - t_0) \right), \quad (4)$$

Here, t_0 is the time at which the peak photon number occurs. A magnified view of a single spike-pulse waveform in the ruby laser and the hyperbolic fitting curve are shown in Fig. 4(b), assuming $\tau = 3.4$ ms and $\tau_p = 2$ ns. A large coefficient of determination of $R^2 = 0.99$ is attained in this case. The intensity probability distribution $P(s)$ for the periodic spiking oscillation corresponding to Fig. 2(a) reaches a minimum at the inflection point, $s_c = s_p \operatorname{sech}^2 \left(\operatorname{arctanh} \frac{1}{\sqrt{3}} \right) = \frac{2}{3} s_p$, as

shown in Fig. 4(c), where $P(s)$ increases monotonically in the region $s > s_c$ [12]

Such a peculiar statistical property relevant to the laser's spiking oscillations strongly suggests that the appropriate self-induced driving force forms so as to cancel the damping force to thereby establish periodic motions preserving the potential energies, $V(u_M) = V(u_m) = E$, over time, as in Fig. 4(a). Ever since the first report in 1968, self-induced pulsations in ruby lasers have drawn interest and have been given a number of plausible explanations in terms of "self-Q-switching" (SQS), which is based on the saturable absorber effect inherent to impurities or reabsorption in the unpumped region, as well as cavity misalignment [6, 17-19].

Here, we investigate the mechanism of self-induced periodic spiking oscillations in the present ruby laser by focusing on the matching between the pump and lasing beam profiles within the ruby crystal. First of all, let us examine the thermal lens effect which modifies the transverse eigenmode to be formed in the laser resonator. The focal length of the thermal lens is given by $f_T = \frac{\pi w_p^2 K_T}{2Q \frac{dn}{dT}}$, $Q = P_{abs} \left(1 - \frac{\nu_l}{\nu_p}\right)$, where P_{abs} is absorbed pump power, ν_p and ν_l are pump and laser optical frequencies, w_p is the average pump spot size in the crystal, and K_T is thermal conductivity [7]. The estimated focal length within the periodic spiking regime is shown by the red curve in Fig. 5(b), assuming $K_T = 0.092 \text{ cal/cm} \cdot \text{C} \cdot \text{sec}$ and $dn/dT = 1.2 \times 10^{-5} / \text{C}$ for ruby crystal.

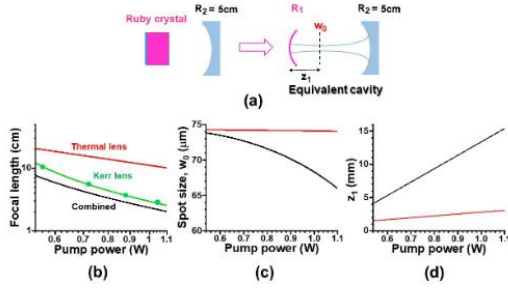


Fig. 5. (a) Equivalent laser-cavity configuration featuring thermal and Kerr lens effects. (b) Pump-dependent focal lengths of thermal, Kerr, and combined lenses. Pump and effective lasing beam spot sizes are assumed to be $72 \mu\text{m}$. (c), (d) Pump-dependent beam waist spot size and its position within the cavity.

In the case of a ruby laser, the complex nonlinear refractive index originates from the light-induced population changes in the excited and ground states of the Cr^{3+} ion [20]. Indeed, a huge *resonance-enhanced* nonlinear refractive index of $n_2 = 1.25 \times 10^{-12} \text{ m}^2/\text{W}$ was reported in an experiment based on the differential interferometric technique using an argon ion laser for the absorption band at 514.5 nm [20], which resulted in self-induced superluminal and subluminal group velocity propagation in the pink ruby [21, 22]. A large amount of frequency chirping was also observed in a Q-switched ruby laser operating at 694 nm [23], which would correspond to a *resonance-enhanced* n_2 -value on the order of $10^{-16} \text{ m}^2/\text{W}$ under lasing conditions, in reference to values of various materials measured by the nonlinear transmittance measurement method [24]. Here, we examine the Kerr-lens effect based on the anomalous dispersion resulting from the population-density changes caused by high-intensity spikes to provide new insights into self-induced spiking behaviors.

The time-dependent focal length of a thin piece (thickness d) of a Kerr lens is given by $f_K = \pi w_e^4 / 8n_2 d P_c(t)$, where w_e is the effective lasing beam spot size and $P_c(t)$ is the circulating intracavity laser power within the ruby crystal [25]. The focal length for the Kerr lens is determined by P_c on the basis of the peak power versus pump power relation shown in Fig. 2(b), assuming 1% transmittance of the output mirror, M_2 , $w_e (\cong w_p) = 72 \mu\text{m}$, and $n_2 d = 10^{-18} \text{ m}^3/\text{W}$.

In Fig. 5(b), the Kerr-lens effect shown by the green curve dominates the thermal-lens effect in the formation of the transverse eigenmode in the laser cavity. The equivalent laser cavity configuration incorporating thermal- and Kerr-lens effects is depicted in Fig. 5(a), where the effective radius of curvature of the coated end surface is given by $R_1 = 2f_c = 2[f_T \cdot f_K / (f_T + f_K)]$, with f_c being the focal length of the combined lens. The resultant pump-dependent beam-waist spot size, w_0 , and its position, z_1 , given by the following equations are shown in Figs. 5(c) and 5(d), respectively.

$$w_0 = \sqrt{\frac{\lambda_0^4}{\pi} \frac{L(R_1 + R_2 - L)(R_1 - L)(R_2 - L)}{R_1 + R_2 - 2L}}, \quad (5)$$

$$z_1 = \frac{L(R_2 - L)}{R_1 + R_2 - 2L}. \quad (6)$$

The lasing mode profiles within the ruby laser crystal calculated using $w_0(z_1)$ values are shown in Fig. 6 for the thermal lens (upper traces) and the combined lens (lower traces), assuming $R_2 = 5 \text{ cm}$ and optical cavity length, $L = 2.5 \text{ cm}$, together with the pump profile. The mode matching between the pump and laser beams and the resultant modal gain for the lasing mode are found to be greatly improved by the Kerr-lens focusing, where the ruby crystal itself acts as a "soft aperture" in the terminology of Kerr-lens mode-locking.

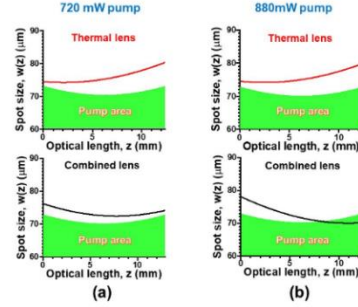


Fig. 6. Spot size variation along the ruby crystal of $l = 7 \text{ mm}$ thickness and $n = 1.77$ refractive index for thermal lens and the combined lens. Pump power: (a) 720 mW , (b) 880 mW .

In 1979, Kubodera and Otsuka introduced the *coupling efficiency*, η_c , which is determined by the overlap integral of the pump beam, $r(x,y,z)$, and the laser beam, $s(x,y,z)$, as [26]

$$\eta_c = \frac{\iiint_{\text{crystal}} r(x,y,z)s(x,y,z)dv^2}{\iiint_{\text{crystal}} r^2(x,y,z)s(x,y,z)dv}, \quad (7)$$

which is related to the slope efficiency as $S_e = \frac{t_2 \nu_l \eta_c \eta_a}{L_c \nu_p}$ (L_c : total cavity loss, t_2 : transmittance of M_2 , η_a : pump absorption coefficient). Here, beam intensities are normalized as $\iiint_{\text{crystal}} r(x,y,x)dv = 1$, $\iiint_{\text{crystal}} s(x,y,z) = nl/L$.

From these relations, the cavity loss, L_c , decreases in proportion to the coupling efficiency given by Eq. (7). The equivalent time-dependent effective loss reduction associated with the time-dependent Kerr-lens effect is $\delta L_c(t)/L_c = 2.3 \times 10^{-2}$ (2.3%) and 5.1×10^{-2} (5.1%) for Fig. 6(a) and Fig. 6(b), respectively. Such a loss modulation provides the laser with the possibility of encouraging spiking operations rather than cw operations through the Kerr-lens mediated balance of the gain and cavity loss, which includes the remaining reabsorption in the unpumped region in Fig. 6.

A similar analysis to that of the periodic loss modulation in a laser Toda potential [12] shows that a spike-mediated driving force, $F_D(t) \propto K \left(\frac{n_2 d}{w_e^2} \right) (P'_c(t) + P_c(t))$, arises, as depicted in Fig. 4(a), in order to reduce dissipative resistive force as if the particle is moving through a viscous medium. In the present ruby laser, the scaling factor, K , is extremely large (1.7×10^6), which ensures pronounced loss modulation.

Additionally, the Kerr lens that mediates the periodic spiking operation requires an initial pulse of sufficient intensity to initiate the effect described above and therefore the spiking sequence. This may not spontaneously occur in cw operation, but the saturable absorption process in the unpumped region is suspected to produce a trigger pulse which initiates spiking.

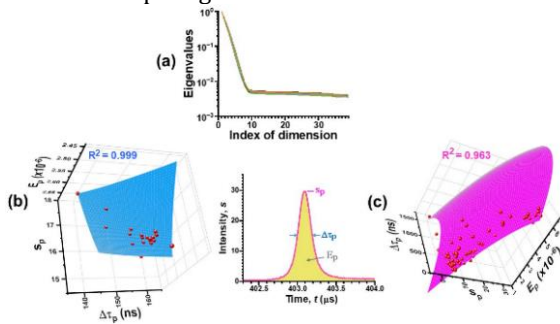


Fig. 7. (a) SDV spectra for chaotic state. 3D statistical graphics for (b) quasi-periodic spiking and (c) chaotic state. Fitting parameter values [a, b, c, d]: (b) $[2.91 \times 10^{-7}, 35.26, -4.05 \times 10^{-9}, -5.97 \times 10^7]$; (c) $[3.80 \times 10^{-7}, 8.41, -4.48 \times 10^{-9}, -4.02 \times 10^6]$.

Finally, let us examine the nonlinear dynamics observed outside the periodic spiking regime. Time-dependent analyses of the singular-value decomposition (SDV) spectra [27] for Fig. 3(b) are shown in Fig. 7(a) for the time interval of data with a length of 4096 bits for each calculation where the next calculation has a shift of 1024 bits. The steep exponential decay in the first segment to the noise floor clearly ensures the existence of chaos in our ruby laser.

An intriguing relation between the peak intensity, s_p , pulse width, $\Delta \tau_p$, and pulse energy (area), E_p , of the spikes depicted in the inset is shown in the 3D statistical graphics for the quasi-periodic spiking (Fig. 7(b)) and chaotic state (Fig. 7(c)). Note that individual pulses with different energies are self-organized to lie on a 2-dimensional parabolic surface $E_p = E_{p,0} + a \cdot s_p + b \cdot \Delta \tau_p + c \cdot s_p^2 + d \cdot \Delta \tau_p^2$ in both cases. The present ruby laser did not show any pure chaotic spiking (hard mode) oscillations contrary to deep external modulations [12]. Occasional appearances of chaotic relaxation oscillations (soft mode) depicted in Fig. 3(b) undermine the self-organization in pure chaotic spiking featuring a large

coefficient of determination of $R^2=0.996$ [12] and result in a degradation to $R^2=0.963$.

References

1. T. H. Maiman, "Stimulated optical radiation in ruby," *Nature* **187**, 493 (1960).
2. M. Birnbaum, P. H. Wendzikowski, and C. L. Fincher, "Continuous-wave nonspiking single-mode ruby lasers," *Appl. Phys. Lett.* **16**, 436 (1970).
3. A. Szabo, "Characteristics of an argon-laser-pumped ruby laser," *J. Appl. Phys.* **46**, 802 (1975).
4. M. Birnbaum, A. W. Tucker, and C. L. Fincher, "Cw ruby laser pumped by an argon-ion laser," *IEEE J. Quantum Electron.* **QE-13**, 808 (1977).
5. T. N. C. Venkatesan and S. L. McCall, "Cw ruby laser pumped by a 5145 Å argon laser," *Rev. Sci. Instrum.* **48**, 539 (1977).
6. A. Szabo, "Repetitive self-Q-switching in a continuously pumped ruby laser," *J. Appl. Phys.* **49**, 533 (1978).
7. R. S. Afzal, W. P. Lin, and Nm. M. Lawandy, "Experimental study of the dynamics of a ruby laser pumped by a cw argon-ion laser," *J. Opt. Soc. Am. B* **6**, 2348 (1989).
8. W. Luhs and B. Wellegehausen, "Diode pumped cw ruby laser," *OSA Continuum* **2**, 184 (2019).
9. W. F. Krupke and J. Zweiback, "High efficiency Gallium Nitride diode pumped cw ruby laser, Proc. of SPIE 11259A (2020).
10. D. Kleinman, "The maser rate equations and spiking," *The Bell System Technical Journal* **43**, 1505 (1964).
11. G. L. Oppo and A. Politi, "Toda potential in laser equations," *Z. Phys. B* **59**, 111 (1985).
12. K. Otsuka and S. Sudo, "Nonlinear dynamics of a self-mixing thin-slice solid-state laser subjected to Doppler-shifted optical feedback," *Phys. Rev. E* **104**, 044203 (2021).
13. M. Toda, "Studies of a non-linear lattice," *Phys. Rep.* **18**, 1 (1975).
14. S. Tarucha and K. Otsuka, "Response of semiconductor laser to deep sinusoidal injection current modulation," *IEEE J. Quantum Electron.* **17**, 810 (1981).
15. K. Kubodera and K. Otsuka, "Spike-mode oscillations in laser-diode pumped LiNdP₄O₁₂ laser," *IEEE J. Quantum Electron.* **17**, 1139 (1981).
16. J.-L. Chern and K. Otsuka, "High-speed picosecond pulse generation in semiconductor lasers with incoherent feedback," *Opt. Lett.* **16**, 1759 (1991); F. Ishiyama, "Bistability of quasi periodicity and period doubling in a delay-induced system," *J. Opt. Soc. Am. B* **16**, 2202 (1999).
17. A. Szabo and L. E. Erickson, "Self-Q-switching of ruby lasers at 77°K," *IEEE J. Quantum Electron.* **4**, 692 (1968).
18. I. Freund, "Self-Q-switching in ruby lasers," *Appl. Phys. Lett.* **12**, 388 (1968).
19. R. J. Collins, L. O. Braun, and D. R. Dean, "A new method of giant pulsing ruby lasers," *Appl. Phys. Lett.* **12**, 392 (1968).
20. H. K. Lee and S. S. Lee, "Measurements of the anisotropic nonlinear refractive-index coefficients of ruby," *Opt. Lett.* **15**, 54 (1990).
21. L.-J. Wang, A. Kuzmich, and A. Dogariu, "Gain-assisted superluminal light propagation," *Nature* **406**, 277 (2000).
22. M. S. Bigelow, N. N. Lepeshkin, and R. W. Boyd, "Observation of ultraslow light propagation in a ruby crystal at room temperature," *Phys Rev Lett* **90**, 113903 (2003).
23. T. Sato, H. Fujiwara, and K. Murata, "Measurement of nonlinear frequency chirp of Q-switched ruby laser," *Appl. Opt.* **20**, 1477 (1981).
24. J.-K. Wang, T.-L. Chiu, C.-H. Chi, and C.-K. Sun, "Nonlinear refraction and absorption measurements with chirped femtosecond laser pulses: experiments and simulations," *J. Opt. Soc. Am. B* **16**, 651 (1999).
25. H. Kogelnik, "Imaging of optical modes-resonators with internal lenses," *Bell Syst. Tech. J.* **44**, 455 (1965).
26. K. Kubodera and K. Otsuka, "Laser performance of a glass-clad LiNdP₄O₁₂ rectangular waveguide," *J. Appl. Phys.* **50**, 6707 (1979).
27. J.-S. Lih, J.-Y. Ko, J.-L. Chern, and I.-M. Jiang, "Deterministic test and noise estimate for a complex time series," *Europhys. Lett.* **40**, 7 (1997).